Catalysis Today xxx (2015) xxx–xxx

Contents lists available at ScienceDirect

Catalysis Today

journal homepage: www.elsevier.com/locate/cattod

Influence of niobium on carbon nanofibres based Cu/ZrO_2 catalysts for liquid phase hydrogenation of CO_2 to methanol

Israf Ud Din[a], Maizatul S. Shaharun[a,*], Duvvuri Subbarao[b], A. Naeem[c], F. Hussain[d]

[a] Department of Fundamental and Applied Sciences, Universiti Teknologi PETRONAS, Malaysia
[b] Department of Chemical Engineering, Universiti Teknologi PETRONAS, Malaysia
[c] National Centre of Excellence in Physical Chemistry, University of Peshawar, Pakistan
[d] Wuhan University of Technology, China

ARTICLE INFO

Article history:
Received 31 December 2014
Received in revised form 9 June 2015
Accepted 29 June 2015
Available online xxx

Keywords:
Methanol synthesis
Slurry reactor
Carbon nanofibres
Copper based
Carbon dioxide conversion
Niobium promoter

ABSTRACT

A series of carbon nanofibres supported $Cu/ZrO_2/Nb_2O_5$ catalyst synthesized by deposition precipitation method were extensively investigated in relation to their performance in hydrogenation of CO_2 to methanol. In order to study the promotion effect of niobium, catalysts were loaded with 0.4, 0.8 and 1.2 wt.% of Nb_2O_5. Incorporation of Nb_2O_5 facilitated copper reduction by exhibiting a shift of highly reduced copper peak to lower temperature. Likewise, surface enrichment of copper was also enhanced by introduction of Nb_2O_5 to the catalysts. Activity studies of Nb_2O_5 doped Cu/ZrO_2 catalysts were evaluated in a slurry reactor with a CO_2/H_2 gas mixture of 1:3 volume ratio, 180°C temperature and 3.0 MPa total pressure. The highest activity was achieved with the incorporation of 0.8 wt.% of Nb_2O_5, illustrating the high degree of CuO crystallization on the surface of catalyst are beneficial for the generation of copper catalyst with enhanced activities.

1. Introduction

Chemical transformation of carbon dioxide into petrochemical products has been extensively investigated over the last few decades [1]. At present, catalytic reduction of CO_2 to methanol is considered as a promising economical route which could contribute to CO_2 mitigation. In fact, current industrial scale methanol synthesis is carried out over $Cu–ZnO/Al_2O_3$ catalysts with a mixture of syngas (CO/H_2) and CO_2 at high operating temperature 300 °C [2]. Furthermore, alumina based catalysts displayed poor activity for CO_2 hydrogenation to methanol due to its high water-affinity [3,4]. These research outcomes have stimulated the development of new catalytic system for hydrogenation of pure CO_2 to methanol. Nevertheless, the lack of probative evidence on the mechanism of CO_2 hydrogenation is the major obstacle for the development of new catalyst formulation [5].

Carbon nanofibres (CNFs) with a high surface area and hydrophobic nature could be a good alternative as a catalyst support for hydrogenation of pure CO_2 to methanol. ZrO_2 doped Cu catalysts have shown promising results for CO_2 hydrogenation [4,6]. Incorporation of promoters like ZnO, Cr_2O_3 and Nb_2O_5 into the Cu/ZrO_2 catalysts have resulted in higher activity and selectivity to methanol in the CO_2 hydrogenation reaction [2,7]. The improved performance of the niobia-supported catalysts was attributed to the formation of new active sites due to the greater interaction of support with the metal atoms [8]. In addition, niobia-supported catalysts were reported to have low acidity property and therefore exhibited better activity and selectivity in hydrogenation reaction of CO and CO_2 [9–11].

In the above context, the specific objectives of this work are to investigate the effect of Nb_2O_5 on the physical, structural and activity of CNFs based Cu/ZrO_2 catalysts in the CO_2 hydrogenation to methanol. The CNFs based Cu/ZrO_2 catalyst was used as reference in the catalytic tests.

2. Experimental

2.1. Functionalization of carbon nanofibres (CNFs)

Surface of CNFs was modified by treating with 35 vol. % nitric acid solution. The refluxing was continued for 16 h at elevated temperature of 90 °C. After refluxing, CNFs were cooled to room temperature and filtered by vacuum filtration. After washing

* Corresponding author.
E-mail address: maizats@petronas.com.my (M.S. Shaharun).

http://dx.doi.org/10.1016/j.cattod.2015.06.019
0920-5861/

several times with distilled water, oxidized CNFs (CNFs-O) were dried overnight in oven at 100 °C.

2.2. Synthesis of Nb_2O_5 doped Cu/ZrO_2/CNF (CZC-Nb) catalysts

Deposition precipitation method was utilized for the synthesis of Nb_2O_5 promoted Cu/ZrO_2/CNF catalysts [12,13]. A series of catalyst containing a constant loading of 15 wt.% Cu and 15 wt.% ZrO_2 with varying Nb_2O_5 content ranged from 0.4, 0.8 and 1.2 wt.% were synthesized. A known quantity of zirconyl nitrate hydrate (SIGMA-ALDRICH, USA) was added gradually to the solution of Cu $(NO_3)_2{\cdot}3H_2O$ (R&M Chemicals, UK). When both nitrate salts were completely dissolved, required quantity of CNFs-O was added to the solution. The suspension was vigorously stirred and heated to 90 °C, then the slurry solution was precipitated with 0.1 g/mL of urea solution. The precipitates were aged at 90 °C for 20 h, cooled and filtered by vacuum filtration. The precipitates were dried in oven at 110 °C for overnight. The catalysts were calcined in N_2 flow at 450 °C for 3 h and labelled as CZC-Nb0.4, CZC-Nb0.8, and CZC-Nb1.2 catalysts. A reference CNF based Cu/ZrO_2 catalyst with a nominal composition of Cu:Zr = 50:50 (wt.%) was prepared using similar technique described above.

2.3. Characterization

PANalytical model Empyrean X-ray diffractometer was employed for phase studies of catalyst components. PANalytical High Score Plus software was used for phase identification. The XRD data were measured at room temperature from 20° to 80° 2θ Bragg angle.

Nitrogen adsorption–desorption isotherms technique was carried out for investigations of catalysts surface area and pore volume using Micrometrics ASAP 2020 [3].

Copper metallic surface area (S_{Cu}), dispersion of Cu (D_{Cu}), average particle size (d_{Cu}) and distribution of Cu content (R_{Cu}) were determined by N_2O chemisorption technique [14–17]. Catalysts were first reduced with H_2 at 500 °C. Reduced samples were cooled in He flow to 60 °C and purged for 30 min. Then N_2O gas was introduced for 1 h. Residual N_2O was flushed out by He flow for 1 h. Finally, the samples were reduced for the second time at 500 °C. Surface area and dispersion of Cu were measured by assuming 1.46×10^{19} Cu_{at}/m^2 surface atomic density and Cu:N_2O = 2 stoichiometry, respectively. Average particle size (d_{Cu}) was obtained by a relationship displayed as follows [3,18,19].

$$d_{Cu}(\text{nm}) = \frac{104}{D_{Cu}(\%)}$$

The distribution of Cu content was estimated by the following equation [20].

$$R_{Cu} = \frac{\text{Cu}^0 \text{ surface area}}{\text{Cu content} \times \text{BET surface area}}$$

Transmission Electron Microscopy (TEM) was used to study morphology and particle size measurement of the catalysts. Zeiss LIBRA 200TEM with accelerating voltage of 200 kV was utilized for this purpose [21].

Temperature Programmed Reduction (TPR) technique was used to study the reduction behaviour of catalyst and metal support interactions. TPDRO1100 MS equipped with thermal conductivity detector (TCD) was used in temperature range of 30–800 °C with heating rate of 10 °C min^{-1}. The analyses were performed in 5 vol.% H_2/N_2 flow with a flow rate of 20 cm^3 min^1.

X-ray photoelectron spectroscopy was utilized to investigate chemical nature and surface composition of Cu. X-ray photoelectron spectroscope (XPS, Thermo-Fisher K-Alpha) equipped with monochromitized AlK source having ultimate energy resolution of ≤0.5 eV was used in XPS studies. Avantage software was used for peak fitting and chemical state identification.

Surface basicity was examined by using CO_2 temperature programmed desorption (CO_2-TPD). Prior to TPD analysis, samples were subjected to temperature of 500 °C for 60 min under inert atmosphere to desorb the surface moisture and other adsorbed molecules. Pre-reduced catalysts were cooled to room temperature and were saturated with pure CO_2. The adsorption of gases was continued for 1 h at 90 °C and physiosorbed molecules were desorbed with He flow. The adsorbed gas was desorbed in temperature range of 40–800 °C. Desorption of CO_2 at relative degree of temperature were quantified by calibrated TCD.

2.4. Catalytic Tests

Activity of catalysts in CO_2 hydrogenation to methanol was evaluated in autoclave slurry reactor slurry reactor (Parr 4593). Prior to the activity studies, the catalysts were reduced for 6 h in H_2 with flow rate of 2000 cm^3/h at 380 °C. A 0.5 grams of reduced sample was suspended in 25 ml of ethanol placed in reaction vessel. The reactor was purged at room temperature and then pressurized with mixture of H_2/CO_2 gases with 3:1 molar ratio to the desirable pressure of 3.0 MPa. The reaction studies were performed at 180 °C. Reaction mixture was agitated by stirrer and a speed of 1300 rpm was selected to avoid mass diffusion constrains. Analysis of reactants and products were carried out on Agilent GC-6890 system chromatograph equipped with a flame ionization and thermal conductivity detectors. Experiments were repeated three time to check for reproducibility. Measurements are in general reproducible within a maximum of 10%. Turnover frequency of methanol was calculated by following formula [22,23]:

$$\text{TOF}_{\text{MeOH}}\,(s^{-1}) = \frac{A \times N_a}{3600 \cdot S_{Cu} \cdot n_a}$$

where A represents methanol activity in mol/g h, N_a is Avogadro's number (6.023×10^{23}), S_{Cu} denotes metallic copper surface area in m^2/g and n_a designates number of Cu atoms in a monolayer ($n_a = 1.469 \times 10^{19}$ atoms/m^2)

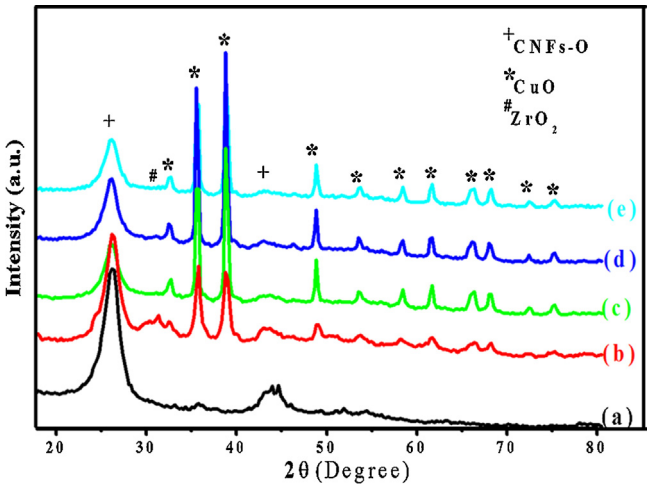

Fig. 1. XRD profile of (a) CNFs-O, (b) CZC, (c) CZC-Nb0.4, (d) CZC-Nb0.8 and (e) CZC-Nb1.2 catalysts.

Please cite this article in press as: I.U. Din, et al., Influence of niobium on carbon nanofibres based Cu/ZrO_2 catalysts for liquid phase hydrogenation of CO_2 to methanol, Catal. Today (2015), http://dx.doi.org/10.1016/j.cattod.2015.06.019

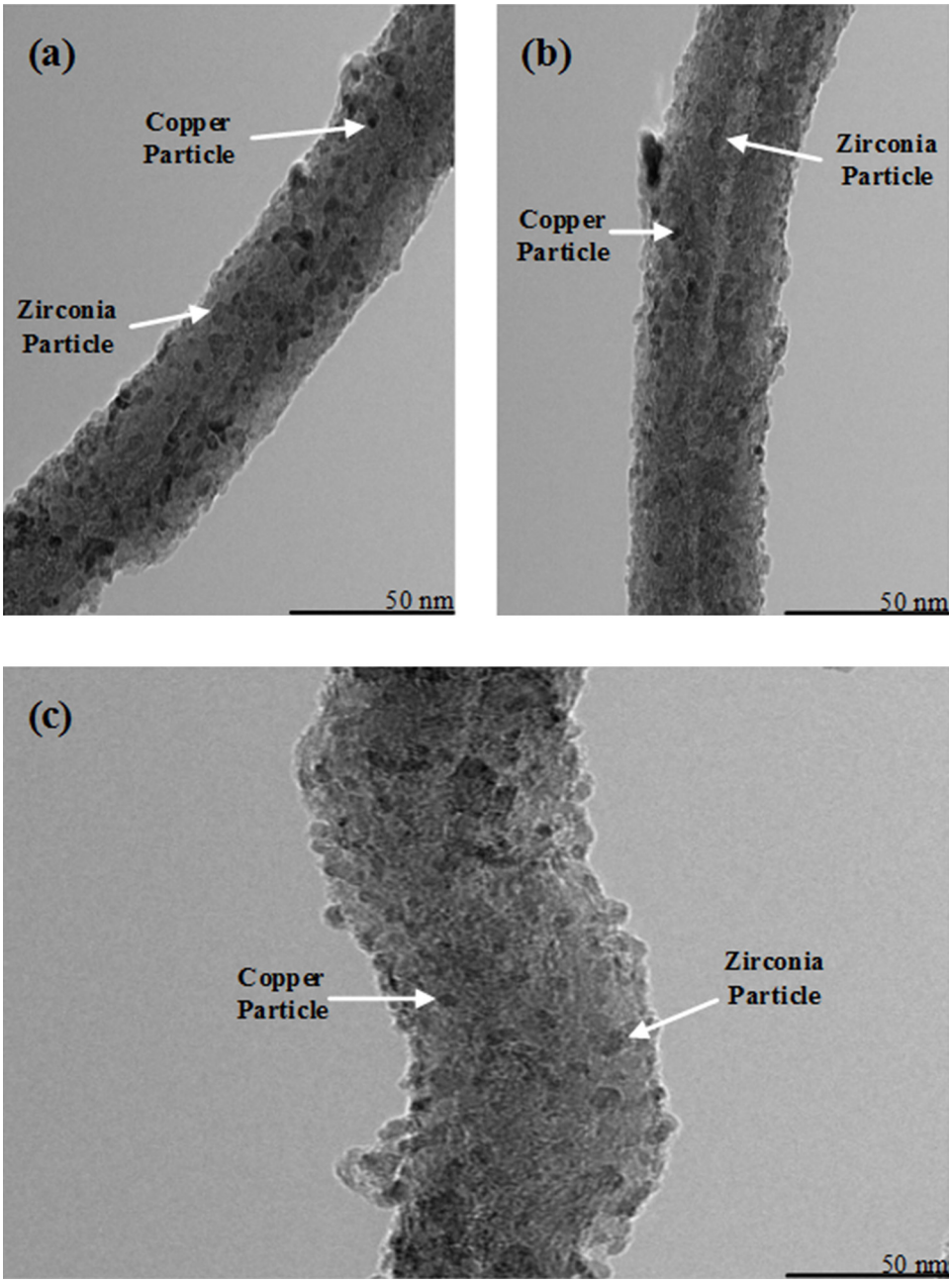

Fig. 2. TEM images of (a) CZC-Nb0.4, (b) CZC-Nb0.8 and (c) CZC-Nb1.2 catalysts.

Table 1
Average particle size of catalyst components.

Catalysts	Copper average particle size (nm)	Zirconia average particle size (nm)
CZC-Nb0.4	4	6
CZC-Nb0.8	5	8
CZC-Nb1.2	7	9

3. Results and discussion

3.1. Catalyst characterization

3.1.1. Phase determination studies

Phase analysis of catalyst components were investigated by XRD technique. XRD profile of Nb promoted CZC catalysts is shown in Fig. 1. For comparison an XRD spectrum of CNFs-O and unloaded CZC catalyst were also included. Hexagonal graphitic planes of CNFs were identified by two prominent peaks at 2θ values of 26° and 44° (JCPDS No. 41-1487). Similarly, diffraction pattern with peaks at 32.6°, 35.5°, 38.7°, 48.8°, 53.6°, 58.3°, 61.67°, 66.4°, 68.1°, 72.3° and 75.1° on 2θ scale was found which is indexed as monoclinic phased tenorite CuO with JCPDS card files No. 48-1548 (a = 4.62 Å, b = 3.43 Å, and c = 5.06 Å). A small diffraction peak around 31° was found in XRD profile, indicating zirconia component of the catalyst. However, it was disappeared with the incorporation of Nb content. This indicates transformation of zirconia to the amorphous phase with the promotion of niobium loading. Highly dispersed or very fine crystalline ZrO_2 (crystallite size < 2 nm) could also be possible reasons. However, peak corresponding to Nb_2O_5 or any Cu-Nb composite was not observed indicating that Nb_2O_5 existed in amorphous or microcrystalline state, which could not

Please cite this article in press as: I.U. Din, et al., Influence of niobium on carbon nanofibres based Cu/ZrO_2 catalysts for liquid phase hydrogenation of CO_2 to methanol, Catal. Today (2015), http://dx.doi.org/10.1016/j.cattod.2015.06.019

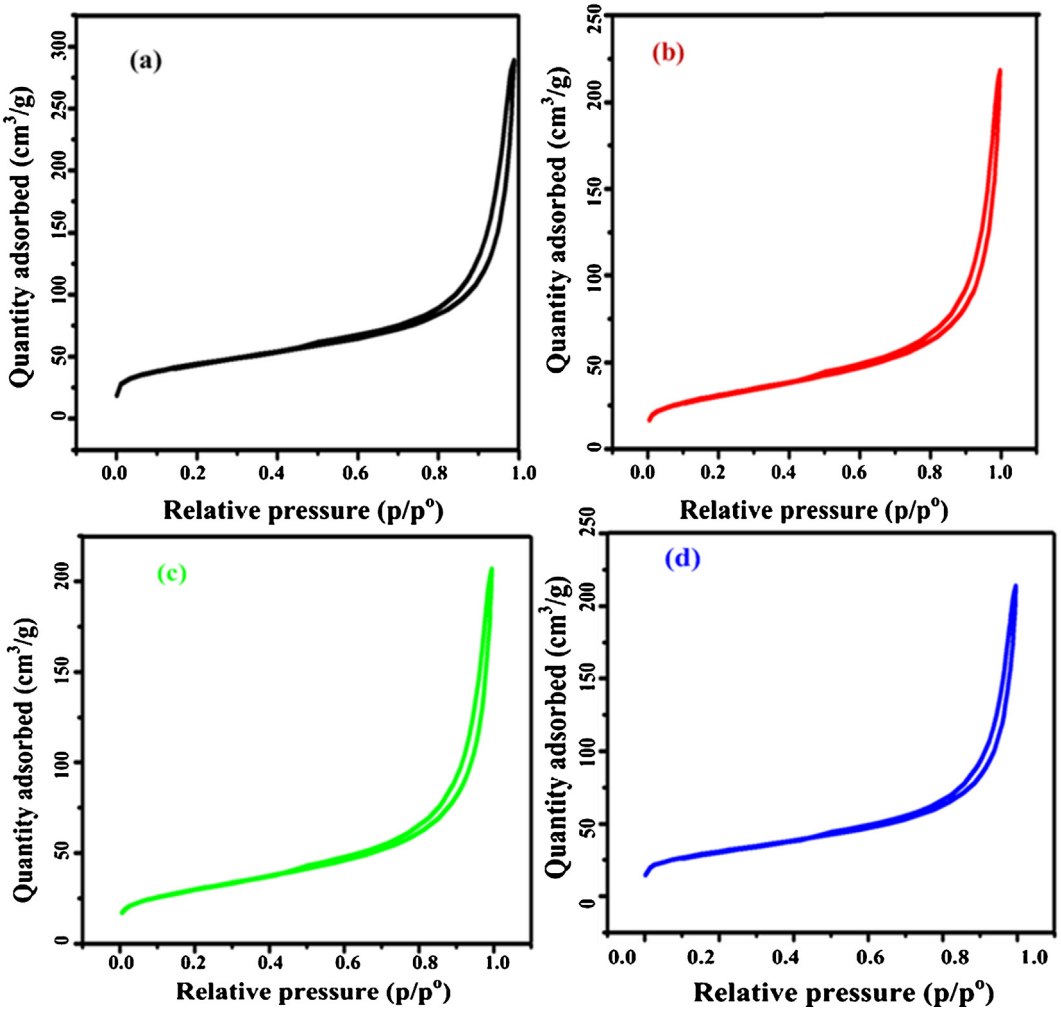

Fig. 3. N_2 adsorption desorption isotherms of (a) CZC, (b) CZC-Nb0.4, (c) CZC-Nb0.8 and (d) CZC-Nb1.2 catalysts.

be detected by XRD technique due to low degree of crystallization. An interesting observation was found in the XRD studies whereby the intensification of CuO peaks is dependent on addition of Nb_2O_5 up to 0.8 wt.% Nb_2O_5 concentration. The increase in CuO peak intensity with increasing Nb_2O_5 loading reflects the growth in crystal size. However, the intensity of CuO peak decreased with further rise in concentration of 1.2 wt.% Nb_2O_5. The decreasing CuO peak intensity with further rise in Nb_2O_5 content indicates the transformation of crystalline CuO to the amorphous form. Such a trend of decreasing CuO peak intensity with increasing copper concentrations was also reported by Rajaram et al. [24].

3.1.2. Morphology investigations

TEM images of CZC and Nb promoted CZC catalysts are presented in Fig. 2. Dark black spherical shaped particles were identified as copper particles whereas tetragonal shaped light coloured particles were recognized as zirconia particles. Particles of copper and zirconia are clearly seen by TEM images. However, Nb_2O_5 particles could not be identified because of their low concentrations. The results demonstrated a homogenous deposition of catalysts particles with low concentrations of Nb_2O_5. Nevertheless, agglomerations of Cu particles were observed when Nb content exceeded 0.8 wt.%. Average particle size of both metal oxides increased with increasing Nb_2O_5 content (Table 1) due to the agglomeration of metal oxides.

Table 2
Textural properties of CZC and Nb promoted CZC catalysts.

Catalyst	Tot. ads. gas (cm^3/g)	S_{BET} (m^2/g)	Pore diameter (nm)	Pore volume (cm^3/g)
CZC	290	155	10.1	0.39
CZC-Nb0.4	220	108	11.3	0.30
CZC-Nb0.8	207	104	11.3	0.29
CZC-Nb1.2	213	105	11.2	0.30

3.1.3. BET surface area and pore size distribution

Nitrogen adsorption-desorption isotherms of CZC and Nb promoted CZC catalysts are shown in Fig. 3. Each catalyst exhibited a typical type-IV isotherm with H4 type hysteresis loops having sharp inflection between p/p^o ranges of 0.90–0.94, indicating mesoporus nature of the synthesized catalysts. The textural properties of CZC catalysts are provided in Table 2. BET surface area decreased remarkably from 155 to 108 m^2/g with the incorporation of 0.4 wt.% of Nb_2O_5 to the CZC catalyst. Although, the surface area reduced with further increase of Nb_2O_5 but the change was not very prominent. The decline of surface area with Nb_2O_5 introduction is supported by a drastic decrease in magnitude of total adsorbed gas from 290 to 220 (cm^3/g) for CZC and CZC-Nb0.8 catalysts, respectively. Similarly, pore volume decreased from 0.39 to 0.29 cm^3/g with the introduction of 0.8 wt.% of Nb_2O_5 to CZC catalysts. The decline in BET surface area and pore volume could be due

Please cite this article in press as: I.U. Din, et al., Influence of niobium on carbon nanofibres based Cu/ZrO_2 catalysts for liquid phase hydrogenation of CO_2 to methanol, Catal. Today (2015), http://dx.doi.org/10.1016/j.cattod.2015.06.019

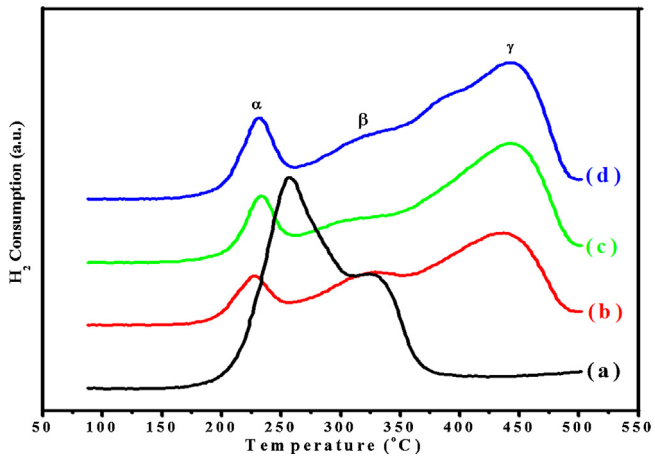

Fig. 4. TPR profile of (a) CZC, (b) CZC-Nb0.4, (c) CZC-Nb0.8 and (d) CZC-Nb1.2 catalysts.

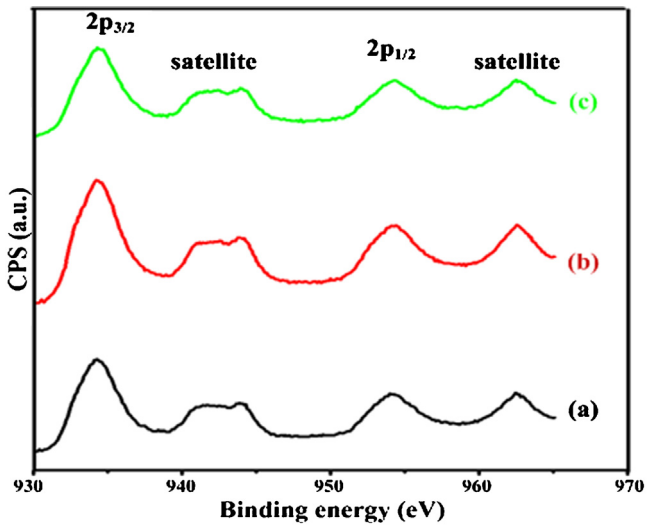

Fig. 5. XPS of Cu 2p of (a) CZC-Nb0.4, (b) CZC-Nb0.8 and (c) CZC-Nb1.2 catalysts.

to pore-filling by the introduction of Nb_2O_5. In contrast, the pore diameter of the catalyst increased with addition of 0.4 wt.% Nb_2O_5 to the CZC catalyst. However, it remained invariant with further addition of Nb_2O_5.

3.1.4. Reducibility studies

The reduction behavior of the catalysts was studied by TPR technique. TPR profile of CZC and Nb-loaded CZC catalysts is presented in Fig. 4. The quantitative evaluation of TPR analysis is shown in Table 3. Two distinct TPR peaks were observed in unprompted CZC catalyst with reduction maxima at 260 and 340 °C and denoted as peak α and peak β, respectively. TPR peak α is recognized as reduction peak due to highly dispersed copper while TPR peak β is ascribed to bulk–like CuO [25]. Similarly, according to López-Suárez et al., peak α is assigned to easily reduced form of Cu^{2+} and peak β correspond to less-reducible CuO [26]. However in concomitant to these two traditional peak, a new broad reduction peak (peak γ) starting at 350 °C with a tail at 490 °C was observed in Nb promoted catalysts. Roma et al. investigated TPR profile of Cu/Nb_2O_5 catalysts and observed a broad peak for CuO reduction around 450 °C [27]. Based on this observation, peak γ in this work could be due to higher interaction of Cu or Cu-Nb_2O_5 composites. Likewise the occurrence of more than two reduction peaks has also been reported in the literature [28]. Nevertheless, an additional reduction peak was observed at 375 °C for CZC catalysts with maximum Nb_2O_5 concentration. TPR peak at the same magnitude of temperature was also recorded by Courtois et al. and attributed to reduction of bulk CuO [29]. Reduction of Nb_2O_5 is generally reported in the temperature range of 800–900 °C in the literature [30–32]. Therefore in the current study, all the reduction peaks attribute to the CuO reduction. This can be further justified by the fact that magnitude of $H_2/Cu < 1$ was recorded for each niobium promoted CZC catalysts as evident in Table 3.

Incorporation of Nb_2O_5 provides interesting changes in TPR profile of CZC catalysts. Position of TPR peak α was shifted from 260 to 230 °C while a lower temperature shift of almost 10 °C was observed in TPR peak β. Shift of peak α to lower temperature with Nb_2O_5 loading suggests that incorporation of Nb_2O_5 facilitated the reduction of Cu^{2+}, in agreement with previous works [33–35]. On the other hand, peak β experienced a higher temperature shift from 340 to 420 °C when CZC catalysts were doped with Nb_2O_5. The shifting of reduction peak is due to the formation of new phase due to strong interaction between Cu and the dopant Nb_2O_5 [36–38]. Guarido et al. reported similar TPR results involving Cu/Nb_2O_5 catalyst used in ethanol reforming and partial oxidation reactions [39]. The results proved that incorporation of Nb_2O_5 in CZC catalysts facilitates the reduction of dispersed Cu at one end but depresses the reducibility of bulk Cu on the other end.

Table 4
XPS data of CZC catalysts with different Nb content.

Sample	Binding energy (eV)		FWHM (eV)		Atomic Cu/Zr ratio
	Cu $2p_{3/2}$	Zr $3d_{5/2}$	Cu $2p_{3/2}$	Zr $3d_{5/2}$	
CZC-Nb0.4	934.10	182.16	3.92	4.57	1.22
CZC-Nb0.8	934.24	182.22	4.11	4.47	1.31
CZC-Nb1.2	934.28	182.18	4.08	4.45	1.21

3.1.5. Metal–metal interaction and surface analysis

Fig. 5 shows the Cu 2p XPS spectra for Nb promoted CZC catalysts. Each catalyst demonstrated Cu $2p_{3/2}$ core electrons peak at 934.4 eV associated with a broad satellite peak around 943 eV. Similarly, core electrons peak for Cu $2p_{1/2}$ was observed at 954 eV accompanied with a shakeup peak around 962 eV. The occurrence of satellite peaks in concomitant to the parental peaks confirms Cu^{2+} as the predominant oxidation state of Cu in all studied catalysts. However, this predominant oxidation state was only observed in the calcined catalysts and not under reaction conditions.

The binding energies of Cu $2p_{3/2}$ and Zr $3d_{5/2}$ core electrons and their full width at half maximum (FWHM) values along with Cu/Zr

Table 3
TPR data of CZC calcined at different temperature.

Sample	H_2 cons. (μmol/g)	H_2/Cu	Red. temp. (°C) peak			H_2 con. (μmol/g) peak		
			α	β	γ	α	β	γ
CZC	2172	0.92	266	340	–	1542	690	–
CZC-Nb0.4	2210	0.94	226	330	437	288	521	1401
CZC-Nb0.8	2239	0.95	235	342	444	291	401	1547
CZC-Nb1.2	2268	0.96	235	355	446	301	517	1450

Please cite this article in press as: I.U. Din, et al., Influence of niobium on carbon nanofibres based Cu/ZrO_2 catalysts for liquid phase hydrogenation of CO_2 to methanol, Catal. Today (2015), http://dx.doi.org/10.1016/j.cattod.2015.06.019

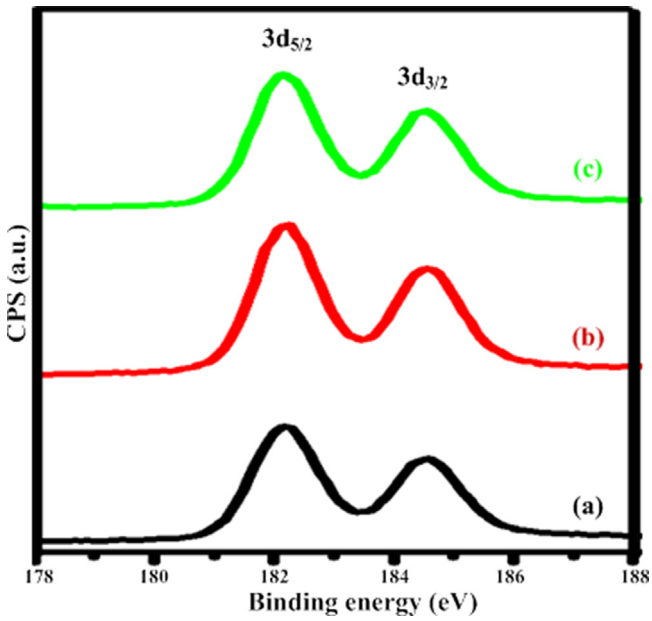

Fig. 6. XPS Zr 3d spectra of (a) CZC-Nb0.4, (b) CZC-Nb0.8 and (c) CZC-Nb1.2 catalysts.

atomic ratio are listed in Table 4. As evident from the tabulated data, binding energy of Cu $2p_{3/2}$ has shifted slightly from 934.10 to 934.24 eV by increasing Nb_2O_5 concentration from 0.4 to 0.8%, respectively. However, substantial variation was not observed with further increase in Nb_2O_5 content. Similarly, position of Zr $3d_{5/2}$ on binding energy scale remained almost invariant for different Nb_2O_5 concentrations. Nevertheless, magnitude of Cu $2p_{3/2}$ FWHM increased slightly from 3.92 to 4.11 eV by increasing Nb_2O_5 concentration from 0.4 to 0.8%. This indicates the formation of two additional weak Cu^{2+}–Cu^{2-} bonding with neighbouring O^{2-} ions, leading to distortion of Cu^{2+} ion coordination symmetry towards a highly distorted octahedral symmetry [40]. On the other hand, FWHM value of Zr $3d_{5/2}$ were not affected by Nb_2O_5 concentration. Therefore information on bonding and nature of Zr^{4+} ions could not be obtained. Furthermore, relative atomic ratio of Cu/Zr increased with by increasing Nb_2O_5 content from 0.4 to 0.8%, suggesting enrichment of surface copper. However, further addition of Nb to the parent catalyst declined the Cu/Zr atomic ratio. This demonstrates depletion of surface Cu and subsequent enrichment of surface Zr content. Agglomeration of Cu could be one of the reasons for surface Cu depletion.

Likewise, XPS profile of Zr 3d of CZC catalysts with different Nb_2O_5 content is depicted in Fig. 6. Zirconium ions were identified by two XPS peaks as Zr $3d_{5/2}$ and Zr $3d_{3/2}$ with binding energies of 182.2 and 184.6 eV, respectively. The presence of two different XPS peaks with 2.4 eV energy gap indicates the existence of two different types of zirconium ions. Lower binding energy peak at 182.2 eV ratifies the existence of Zr^{4+} as ZrO_2 whereas higher binding energy peak at 184.6 eV represents Zr^{2+} species [41].

Cu $2p_{3/2}$ peak of each catalyst was resolved into different peaks to identify the different Cu species and is displayed in Fig. 7. Cupric ion can easily be recognized due to its characteristic coupling phenomenon between unpaired electrons. However, magnitudes of binding energies of Cu^0 and Cu^+ are so closed that the two peaks overlap each other, hence these two Cu species could not be differentiated. In the current study, higher energy Cu $2p_{3/2}$ peak observed at 933.7 eV was attributed to Cu^{2+} ion while a low energy peak centred at 932.7 eV was assigned to Cu^+ ion. The appearance of two different CuO species by XPS analysis strongly support the H_2-TPR findings where step-wise reduction of CuO was detected.

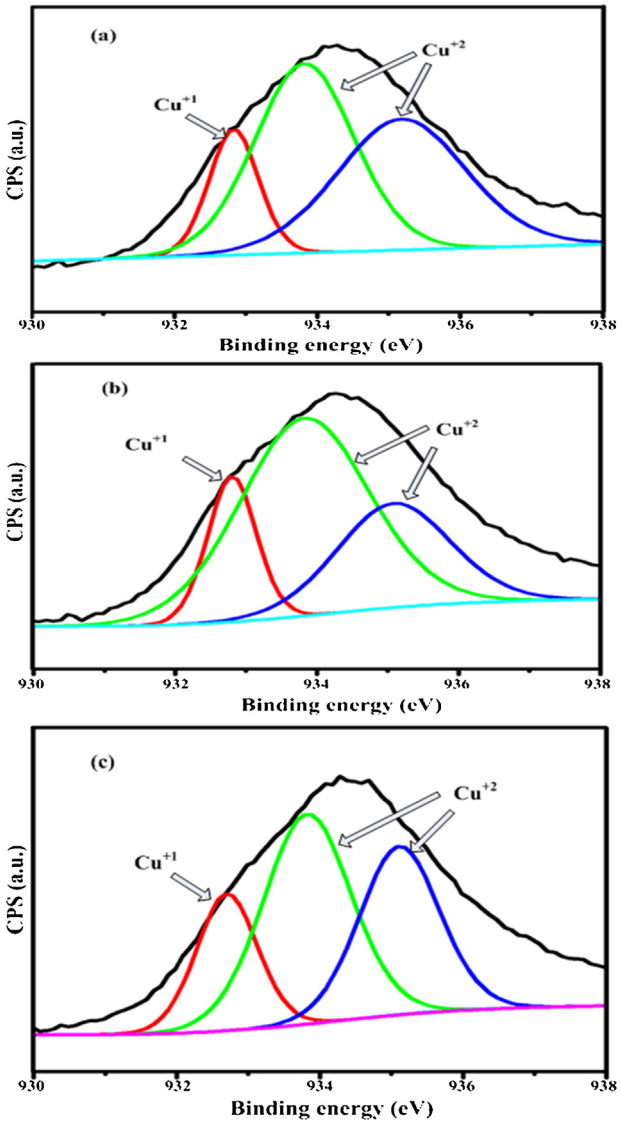

Fig. 7. XPS Cu 2p peak fitting curves of (a) CZC-Nb0.4, (b) CZC-Nb0.8 and (c) CZC-Nb1.2 catalysts.

XPS profile of Nb 3d core electrons of Nb promoted CZC catalysts is displayed in Fig. 8. Two major peaks were observed for Nb 3d region, Nb $3d_{5/2}$ peak centred at 207 eV and Nb $3d_{3/2}$ peak originated at 210 eV. In order to identify the different forms of niobium oxide, Nb 3d region was deconvoluted into six different peaks.

Generally metallic Nb is characterized by its XPS peak at 202 eV which was not found in the current case, indicating the absence of Nb metal. However, XPS analysis revealed the existence of Nb in different oxygenated forms. The two main XPS peaks at 207.1 and 209.7 eV were recognized as $Nb^{5+}(2)$ peaks, indicating the presence of Nb_2O_5 [42,43]. Another major contribution of niobium oxide form was recognized by $Nb^{5+}(1)$ peak with binding energies of 206.5, 209.16 and 210.09 eV indicating NbO_6 octahedra. Besides, the existence of these two oxides, XPS peak for NbO_4 was manifested by a small shoulder at 208.1 eV. [44]. The contribution of each oxide to the total Nb_2O_5 was calculated and listed in Table 5. Incorporation of Nb_2O_5 content affected the contribution of each oxide. Relative percentage of Nb_2O_5 increased whereas contribution of NbO_6 declined with increasing Nb content from 0.4 to 0.8 wt.%. In contrast, the opposite trend was observed when the Nb content was further increased from 0.8 to 1.2 wt.%. However, contribution

Please cite this article in press as: I.U. Din, et al., Influence of niobium on carbon nanofibres based Cu/ZrO_2 catalysts for liquid phase hydrogenation of CO_2 to methanol, Catal. Today (2015), http://dx.doi.org/10.1016/j.cattod.2015.06.019

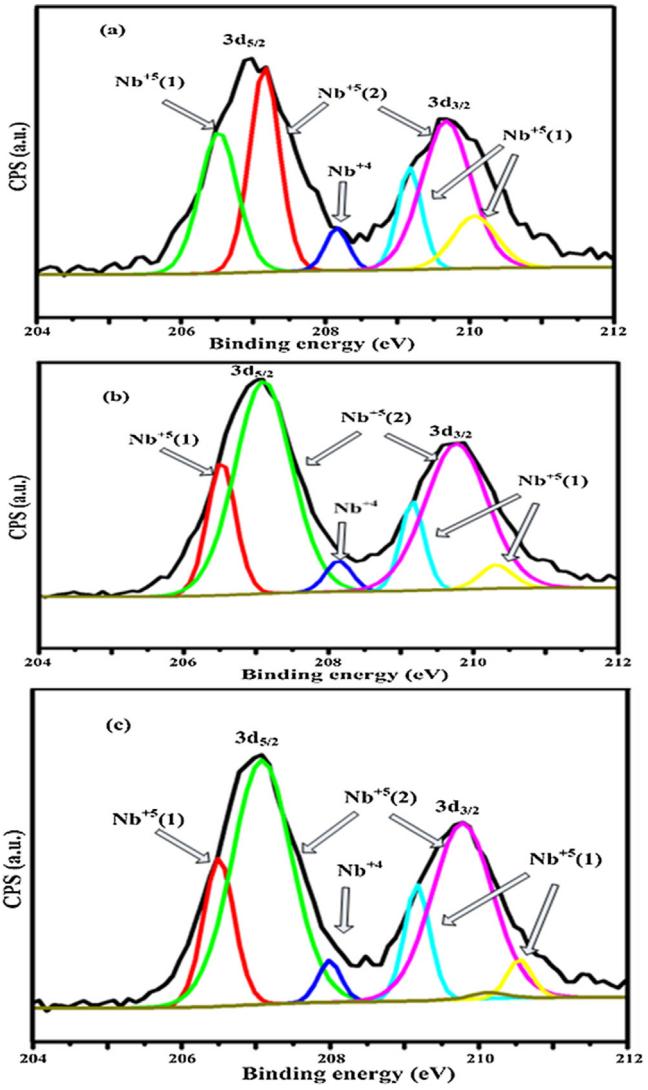

Fig. 8. XPS Nb 3d peak fitting curves of (a) CZC-Nb0.4, (b) CZC-Nb0.8 and (c) CZC-Nb1.2 catalysts.

Table 5
Contribution of each oxide to total niobium oxide.

Catalyst	i_A (%)		
	Nb_2O_5	NbO_6	NbO_4
CZC-Nb0.4	68	28	4
CZC-Nb0.8	74	23	3
CZC-Nb1.2	71	26	3

i_A (%) represents the ratio of $A_i/\Sigma A_i$ (A_i is the area of each peak).

of NbO_4 remained almost invariant throughout the range of Nb loadings.

3.1.6. Basicity studies

Fig. 9 shows CO_2 TPD profile of Nb promoted CZC catalysts. Basic sites were found in temperature range of 250–650 °C. Basic sites

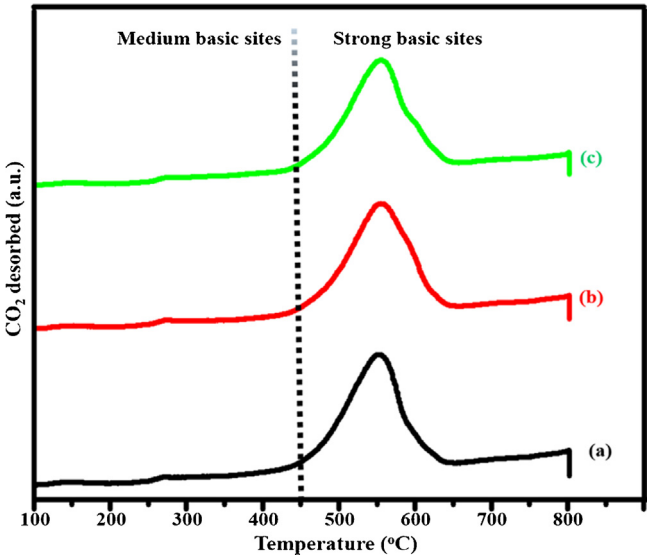

Fig. 9. CO_2-TPD profile of (a) CZC-Nb0.4, (b) CZC-Nb0.8 and (c) CZC-Nb1.2 catalysts.

Table 7
N_2O chemisorption data of un-promoted and Nb oxide promoted catalysts.

Sample	S_{Cu} (m^2/g)	D_{Cu} (%)	d_{Cu} (nm)	R_{Cu}
CZC	8.0	22.0	4.7	0.34
CZC-Nb0.4	14.4	15.8	6.6	0.88
CZC-Nb0.8	15.9	17.2	6.0	1.00
CZC-Nb1.2	15.4	16.5	6.3	0.97

were classified as medium basic sites (below 450 °C) and strong basic sites (above 450 °C). Irrespective of the Nb concentrations, basic sites were predominantly found in the higher temperature region. This implies that strength of basic sites is not affected by variation in Nb content.

Total number of basic sites, their densities and relative distribution is provided in Table 6. Total number of basic sites remained almost constant throughout the range of Nb_2O_5 concentration. Similarly the densities of total basic sites were also found invariant with the variation of Nb_2O_5 concentrations. Magnitude of medium basic sites increased moderately when the concentration of Nb_2O_5 increased from 0.4 to 0.8 wt.%. However the magnitude of medium basic sites declined with further addition of Nb_2O_5 content beyond 0.8 wt.%.

3.2. Chemisorption studies

The surface area of metallic copper (S_{Cu}), Cu dispersion (D_{Cu}), average particle size (d_{Cu}) and relative distribution of metallic copper (R_{Cu}) measured by N_2O chemisorption are presented in Table 7. As evident from the tabulated data, increase in Nb_2O_5 content has a marked influence on the surface properties of Cu. The surface area of metallic copper increased progressively with incorporation of Nb_2O_5 content in the parent catalyst and a maximum S_{Cu} of 15.9 m^2/g was obtained for CZC-Nb0.8 catalyst. However, the S_{Cu} decreased with further rise in concentration of Nb_2O_5 content beyond 0.8 wt.%. Unlike S_{Cu}, dispersion of Cu (D_{Cu}) was adversely

Table 6
CO_2 TPD data of Nb promoted CZC catalysts.

Catalyst	Number of total basic sites (μmol/g cat)	Density of total basic sites (μmol/m^2)	Medium basic sites (μmol/g cat)	Strong basic sites (μmol/g cat)
CZC-Nb0.4	333	1.51	33	300
CZC-Nb0.8	331	1.60	39	292
CZC-Nb1.2	334	1.57	34	300

Please cite this article in press as: I.U. Din, et al., Influence of niobium on carbon nanofibres based Cu/ZrO_2 catalysts for liquid phase hydrogenation of CO_2 to methanol, Catal. Today (2015), http://dx.doi.org/10.1016/j.cattod.2015.06.019

Table 8
Activity data of CZC and Nb promoted CZC catalysts.

Catalyst	Methanol activity (g/kg cat h)	CO_2 conversion (%)	Methanol selectivity (%)	TOF_{MeOH} (s^{-1})
CZC	32	14	75	1.42
CZC-Nb0.4	37	10	89	0.92
CZC-Nb0.8	40	9	87	0.89
CZC-Nb1.2	38	8	88	0.88

Table 9
Comparative study of the current catalyst for CO_2 hydrogenation to methanol with the literature data.

Catalyst	T (°C)	P (bar)	Methanol activity (g/kg h)	CO_2 conversion (%)	Reference
$CuO/ZnO/Al_2O_3$	170	30	20	5.8	[7]
Pd/Zn/CNTs	250	30	37	6.3	[42]
$Pd/ZnO/Al_2O_3$	250	30	24	4.4	[42]
PdZnO/AC	250	30	28	4.9	[42]
Ag/ZrO_2	230	80	27	–	[36]
$Cu/B_2O_3/ZrO_2$	250	20	57	16	[41]
$Cu/Ga_2O_3/ZrO_2$	250	20	62	13.7	[41]
$Cu/ZnO/ZrO_2$	220	80	40	2	[40]
$Au/ZnO/ZrO_2$	220	80	19	2	[40]
$Ag/ZnO/ZrO_2$	220	80	15	2	[40]
Cu/ZrO_2	200	9	23	1.7	[47]
$Cu/ZrO_2/ZnO$	200	9	48	5.8	[47]
CZC-Nb0.8	180	30	40	9	Present work

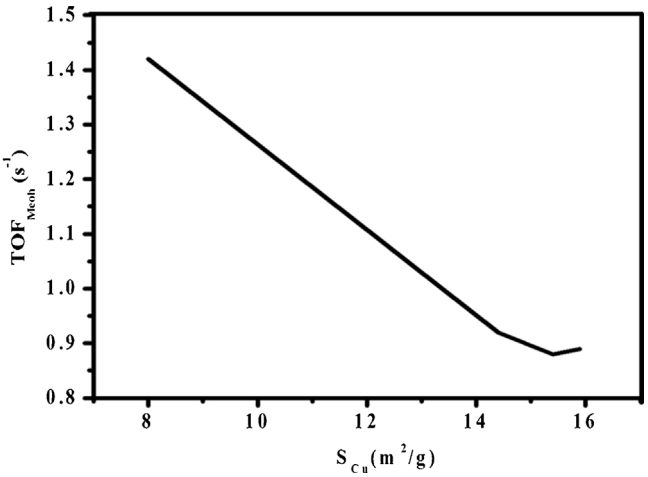

Fig. 10. Correlation of S_{Cu} and methanol TOF.

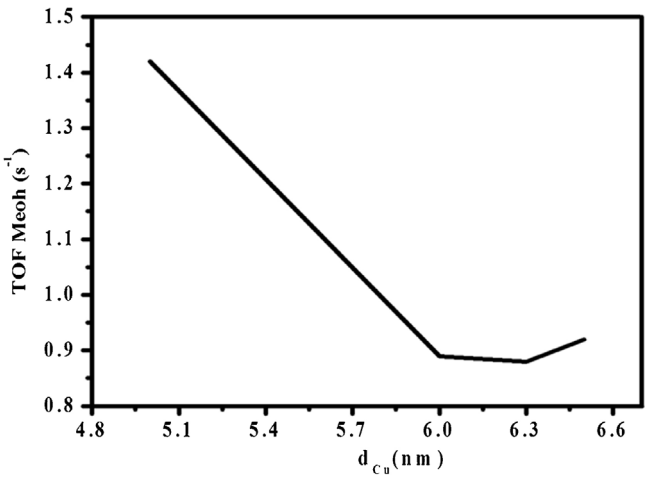

Fig. 11. Correlation of d_{Cu} and methanol TOF.

affected by incorporation of Nb_2O_5 to the parent CZC catalyst. The D_{Cu} increased from 15.8% to 17.2% with the addition of Nb_2O_5 of 0.4 to 0.8 wt.%. However, it remained almost invariant with further addition of Nb_2O_5. On the other hand, the copper particle size was less affected by variation of Nb_2O_5 content. Distribution of surface copper (R_{Cu}) increased to a maximum with the incorporation of 0.8 wt.% Nb_2O_5.

3.3. Catalytic tests

Table 8 displays the variation of catalysts performance as a function of Nb_2O_5 loading. Methanol synthesis rate increased from 32 to 37 (g/kg cat h) with the incorporation of 0.4 wt.% Nb_2O_5 to the CZC parent catalyst. Further addition of Nb_2O_5 to 0.8 wt.% improved the catalysts activity to 40 (g/kg cat h). Nevertheless, methanol synthesis rate decreased with further incorporation of Nb_2O_5 content (1.2 wt.%). The increment in methanol synthesis rate by Nb_2O_5 promotion could be due to the ease of Cu reduction as indicated by TPR studies. Likewise the increase in methanol synthesis rate could be justified by the improvement of methanol selectivity as a function of Nb_2O_5 introduction to the parent catalyst. On the other hand, CO_2 conversion was adversely affected by Nb_2O_5 addition. Apart from methanol, ethane, hexane and carbon monoxide were also found as by-products in the GC chromatogram of the reaction mixture.

In terms of methanol synthesis, a comparative study of the activity data of this novel catalyst with the reported literature revealed that the current Nb_2O_5 promoted CZC catalysts showed higher activity for methanol yield and CO_2 conversion as compared to that recorded by Shaharun et al. over $Cu/ZnO/Al_2O_3$ and Sloczynski et al. over $Ag/ZnO/ZrO_2$ and $Au/ZnO/ZrO_2$ catalysts [7,45]. Similarly, the results obtained in this study were very much comparable in terms of methanol yield and CO_2 conversion to the work of Liu et al., for CO_2 hydrogenation over $Cu/Ga_2O_3/ZrO_2$ catalysts [46]. Furthermore, a comparable activity data for methanol synthesis were reported by Liang et al. for carbon nanotube-supported Pd/ZnO catalysts [47]. A detailed comparative study of the current catalyst for CO_2 hydrogenation to methanol with the literature is displayed in Table 9.

Incorporation of 0.4 wt.% of Nb_2O_5 led to decline of CO_2 conversion from 14 to 10%. However, CO_2 conversion remained almost constant by further increase in Nb_2O_5 content. From the activity pattern, it could be inferred that Nb_2O_5 promotion has a supporting effect on the methanol selectivity. Similar observations were also reported by Passos et al. in the *n*-heptane conversion to olefins

Please cite this article in press as: I.U. Din, et al., Influence of niobium on carbon nanofibres based Cu/ZrO_2 catalysts for liquid phase hydrogenation of CO_2 to methanol, Catal. Today (2015), http://dx.doi.org/10.1016/j.cattod.2015.06.019

using Nb_2O_5 promoted platinum catalyst [48]. Similarly turnover frequency (TOF) of methanol synthesis reduced significantly from 1.42 to 0.92 s^{-1} by incorporation of 0.4 wt.% Nb_2O_5.

In order to investigate the role of S_{Cu} in CO_2 hydrogenation to methanol, a graph was plotted between S_{Cu} and TOF of methanol formation. As evident from Fig. 10, TOF decreased with increasing copper surface area. Generally activity of the copper based catalysts increases linearly with increasing S_{Cu}. However conflicting results have also been reported in the literature [49,50]. The results obtained in the current study reveal that S_{Cu} is not the only factor to regulate the catalysts activity. Apart from S_{Cu} different factors affecting the catalytic activity have been proposed by different researchers. The higher selectivity of the Nb_2O_5 promoted catalyst could be due to the role of Nb_2O_5 to hold more metallic Cu in promoted CZC catalyst. This can also be justified by increasing S_{Cu} with the introduction of Nb_2O_5 to the parent CZC catalyst. Similar observations were reported by Yoshihara and Cambell for methanol synthesis over Cu/ZnO catalysts [51].

To study structure sensitivity behavior of the CO_2 hydrogenation, a graph was plotted between copper particles size (d_{Cu}) and TOF of methanol formation. As indicated by Fig. 11, a sharp decline was observed in magnitude of TOF with increasing d_{Cu} from 5 to 6 nm. Nevertheless, it remained almost constant with further growth of d_{Cu}. This is because of the small variation of d_{Cu} as a consequent of Nb_2O_5 addition.

4. Conclusion

CZC catalysts with different concentrations of Nb_2O_5 were synthesized to study the promoting effect of Nb. The addition of Nb_2O_5 significantly modified the XRD spectra of the CZC catalyst. Increasing the Nb_2O_5 content, increased the intensity of the CuO peak which reflect the growth of the Cu crystal size. When niobium oxide was incorporated into the CZC catalyst, the small diffraction peak around 31° suggested that the zirconia crystal was transformed to the amorphous phase at 0.4 to 1.2 wt.% Nb_2O_5 loading. In addition, the shift of TPR peak α to lower temperature with Nb_2O_5 loading suggests that incorporation of Nb_2O_5 facilitated the reduction of dispersed Cu. Physicochemical and activity data revealed CZC catalysts with 0.8 wt.% Nb_2O_5 content is the most efficient catalyst in the hydrogenation of CO_2 to methanol in a slurry reactor. High methanol activity up to 40 g/kg.cat.h can be achieved at low temperature and total pressure of 453 K and 30 bar, respectively.

Acknowledgements

This work was supported by Ministry of Science, Technology and Innovation (MOSTI) and Government of Malaysia under the Research Project No. 03-02-02-SF0084, Ministry of Higher Education Malaysia, FRGS No: FRGS/1/2011/SG/UTP/02/13 and Universiti Teknologi PETRONAS, Malaysia.

References

[1] W. Cai, P.R. de la Piscina, J. Toyir, N. Homs, Catal. Today 242 (Part A) (2015) 193–199.
[2] G. Bonura, F. Arena, G. Mezzatesta, C. Cannilla, L. Spadaro, F. Frusteri, Catal. Today 171 (2011) 251–256.
[3] F. Arena, K. Barbera, G. Italiano, G. Bonura, L. Spadaro, F. Frusteri, J. Catal. 249 (2007) 185–194.
[4] C. Yang, Z. Ma, N. Zhao, W. Wei, T. Hu, Y. Sun, Catal. Today 115 (2006) 222–227.
[5] F. Arena, G. Mezzatesta, G. Zafarana, G. Trunfio, F. Frusteri, L. Spadaro, Catal. Today 210 (2013) 39–46.
[6] P. Gao, F. Li, F. Xiao, N. Zhao, W. Wei, L. Zhong, Y. Sun, Catal. Today 194 (2012) 9–15.
[7] S. Shaharun, M.S. Shaharun, D. Mohamad, M.F. Taha, AIP Conf. Proc. 1621 (2014) 3–9.
[8] Z. Hu, K. Kunimori, T. Uchijima, Appl. Catal. 69 (1991) 253–268.
[9] T. Iizuka, Y. Tanaka, K. Tanabe, J. Mol. Catal. A: Chem. 17 (1982) 381–389.
[10] A. Frydman, D.G. Castner, C.T. Campbell, M. Schmal, J. Catal. 188 (1999) 1–13.
[11] M. Schmal, A. Frydman, J. Catal. 188 (1999) 1–13.
[12] M.L. Toebes, M.K. van der Lee, L.M. Tang, M.H. Huis in't Veld, J.H. Bitter, A.J. van Dillen, K.P. de Jong, J. Phys. Chem. B 108 (2004) 11611–11619.
[13] M.K. van der Lee, J. van Dillen, J.H. Bitter, K.P. de Jong, JACS 127 (2005) 13573–13582.
[14] X.-L. Du, Q.-Y. Bi, Y.-M. Liu, Y. Cao, H.-Y. He, K.-N. Fan, Green Chem. 14 (2012) 935–939.
[15] G. Sengupta, D.K. Gupta, M.L. Kundu, S.P. Sen, J. Catal. 67 (1981) 223–225.
[16] T.J. Osinga, B.G. Linsen, W.P. van Beek, J. Catal. 7 (1967) 277–279.
[17] B. Dvořák, J. Pašek, J. Catal. 18 (1970) 108–114.
[18] J.W. Evans, M.S. Wainwright, A.J. Bridgewater, D.J. Young, Appl. Catal. 7 (1983) 75–83.
[19] G. Bonura, M. Cordaro, C. Cannilla, F. Arena, F. Frusteri, Appl. Catal. B 152–153 (2014) 152–161.
[20] J. Agrell, M. Boutonnet, I. Melián-Cabrera, J.L.G. Fierro, Appl. Catal. A 253 (2003) 201–211.
[21] C. Sievers, O. Jiménez, R. Knapp, X. Lin, T.E. Müller, A. Türler, B. Wierczinski, J.A. Lercher, J. Mol Catal. A: Chem. 279 (2008) 187–199.
[22] H. Ahouari, A. Soualah, A. Le Valant, L. Pinard, P. Magnoux, Y. Pouilloux, React. Kinet. Catal. Lett. 110 (2013) 131–145.
[23] Q. Sun, Y.-L. Zhang, H.-Y. Chen, J.-F. Deng, D. Wu, S.-Y. Chen, J. Catal. 167 (1997) 92–105.
[24] K. Rajaram, E. Savarimuthu, S. Arumugam, Chem. Sci. Rev. Lett. 2 (2014) 626–629.
[25] W.P. Dow, T.J. Huang, J. Catal. 147 (1994) 322–332.
[26] F.E. López-Suárez, A. Bueno-López, M.J. Illán-Gómez, Appl. Catal. B 84 (2008) 651–658.
[27] M.N.S.C. Roma, D.S. Cunha, G.M. Cruz, A.J.G. Cobo, Braz. J. Chem. Eng. 17 (2000) 937–946.
[28] X.-m.Z. Gong-Xin Qi, Jin-hua Fei, Zhao-yin Hou, Indian J. Chem. 40A (2001) 588–593.
[29] V.P.X. Courtois, M. Primet, G. Bergeret, Stud. Surf. Sci. Catal. 130 (2000) 1031–1036.
[30] F.d.O. Cantão, W.d.C. Melo, L.C.A. Oliveira, A.R. Passos, A.C.d. Silva, Quim. Nova 33 (2010) 528–531.
[31] M. Ziolek, Catal. Today 78 (2003) 47–64.
[32] C.G. Alonso, A.C. Furtado, M.P. Cantao, O.A.A. Dos Santos, N.R.C. Fernandes-Machado, Int. J. Hydrogen Energy 34 (2009) 3333–3341.
[33] S. Esposito, M. Turco, G. Bagnasco, C. Cammarano, P. Pernice, A. Aronne, Appl. Catal. A 372 (2010) 48–57.
[34] P.H. Matter, D.J. Braden, U.S. Ozkan, J. Catal. 223 (2004) 340–351.
[35] L.C. Wang, Q. Liu, M. Chen, Y.M. Liu, Y. Cao, H.Y. He, K.N. Fan, J. Phys. Chem. C 111 (2007) 16549–16557.
[36] C.G. Alonso, A.C. Furtado, M.P. Cantão, O.A. Andreo dos Santos, N.R. Camargo Fernandes-Machado, Int. J. Hydrogen Energy 34 (2009) 3333–3341.
[37] F.B. Noronha, M. Schmal, M. Primet, R. Frety, Appl. Catal. 78 (1991) 125–139.
[38] M.P. Maia, M.A. Rodrigues, F.B. Passos, Catal. Today 123 (2007) 171–176.
[39] C.E.M. Guarido, D.V. Cesar, M.M.V.M. Souza, M. Schmal, Catal. Today 142 (2009) 252–257.
[40] Y.-W. Suh, S.-H. Moon, H.-K. Rhee, Catal. Today 63 (2000) 447–452.
[41] R. Grabowski, J. Słoczyński, M. SÍiwa, D. Mucha, R.P. Socha, M. Lachowska, J. Skrzypek, ACS Catal. 1 (2011) 266–278.
[42] N. Özer, T. Barreto, T. Büyüklimanli, C.M. Lampert, Sol. Energy Mater. Sol. Cells 36 (1995) 433–443.
[43] C. Zhou, Y. Zhao, L. Shang, Y. Cao, L.-Z. Wu, C.-H. Tung, T. Zhang, Chem. Commun. 50 (2014) 9554–9556.
[44] G. Zhang, X. Zou, J. Gong, F. He, H. Zhang, S. Ouyang, H. Liu, Q. Zhang, Y. Liu, X. Yang, B. Hu, J. Mol. Catal. A: Chem. 255 (2006) 109–116.
[45] J. Słoczyński, R. Grabowski, A. Kozłowska, P. Olszewski, J. Stoch, J. Skrzypek, M. Lachowska, Appl. Catal. A 278 (2004) 11–23.
[46] X.-M. Liu, G.Q. Lu, Z.-F. Yan, Appl. Catal. A 279 (2005) 241–245.
[47] X.-L. Liang, X. Dong, G.-D. Lin, H.-B. Zhang, Appl. Catal. B: Environ. 88 (2009) 315–322.
[48] F.B. Passos, D.A.G. Aranda, R.R. Soares, M. Schmal, Catal. Today 43 (1998) 3–9.
[49] H. Ahouari, A. Soualah, A. Le Valant, L. Pinard, P. Magnoux, Y. Pouilloux, React. Kinet. Mech. Catal. 110 (2013) 131–145.
[50] H. Berndt, V. Briehn, S. Evert, Appl. Catal. A 86 (1992) 65–69.
[51] J. Yoshihara, C.T. Campbell, J. Catal. 161 (1996) 776–782.

Please cite this article in press as: I.U. Din, et al., Influence of niobium on carbon nanofibres based Cu/ZrO_2 catalysts for liquid phase hydrogenation of CO_2 to methanol, Catal. Today (2015), http://dx.doi.org/10.1016/j.cattod.2015.06.019